

Leading corrections to local approximations II (with turning points)

Raphael F. Ribeiro

Department of Chemistry and Biochemistry, University of California, San Diego, CA, 92093

Kieron Burke

Department of Chemistry, University of California, Irvine, CA 92697

Quantum corrections to Thomas-Fermi (TF) theory are investigated for noninteracting one-dimensional fermions with known uniform semiclassical approximations to the density and kinetic energy. Their structure is analyzed, and contributions from distinct phase space regions (classically-allowed versus forbidden at the Fermi energy) are derived analytically. Universal formulas are derived for both particle numbers and energy components in each region. For example, in the semiclassical limit, exactly $(6\pi\sqrt{3})^{-1}$ of a particle leaks into the evanescent region beyond a turning point. The correct normalization of semiclassical densities is proven analytically in the semiclassical limit. Energies and densities are tested numerically in a variety of one-dimensional potentials, especially in the limit where TF theory becomes exact. The subtle relation between the pointwise accuracy of the semiclassical approximation and integrated expectation values is explored. The limitations of the semiclassical formulas are also investigated when the potential varies too rapidly. The approximations are shown to work for multiple wells, except right at the mid-phase point of the evanescent regions. The implications for density functional approximations are discussed.

PACS numbers: 03.65.Sq, 05.30.Fk, 31.15.xg, 71.15.Mb

I. INTRODUCTION

While the popularity of density functional theory (DFT) has never been higher [1], the lack of a systematic approach to the construction of approximate exchange-correlation functionals or even orbital-free kinetic energy functionals remains an outstanding issue confronted by practitioners and developers of the theory alike. The closest to a systematic approach might be the decades-long work of Perdew and co-workers, which recently yielded a highly promising meta-generalized gradient approximation called SCAN, but only after 20 years of research, and including norms which are used to fix parameters in the approximation [2].

Semiclassical approximations have inspired the development of density functional methods from the start. The first density functional approximation is given by Thomas-Fermi (TF) theory [3, 4]. It may be regarded as a classical limit of quantum mechanics. As such, it has been proved to be a universal limit for the quantum mechanics of nonrelativistic matter [5]. More recently, it has been conjectured that the analogous statement in Kohn-Sham DFT, that the local density approximation for both exchange and correlation, also becomes relatively exact in this limit [6]. Therefore, it is unsurprising the most successful density functional approximations reduce to local density approximations in the limit where the predictions according to the latter become exact.

Over the past decade [6–14], our group has pursued the connection between semiclassical approximations and DFT. Much of the work can be classified as being in one of two camps: they are either limited to one-dimension, or have a general scope. The advantage of one dimension is that semiclassical approximations to wave functions are long known [15–18]. Thus more explicit progress, includ-

ing analytic results are possible in 1D, and suggest both the greatest power and limitations of this approach more generally. Earlier work made an even greater simplification, by employing box boundary conditions to avoid the singularities associated with turning points [10]. More recently, at least in the case of densities and kinetic energy densities, a semiclassical approximation was derived [13] which is uniformly asymptotic in space, i.e., suffers no singularities, while capturing the leading corrections to TF results at every point. A brief account appeared in Ref. [13], while a more detailed mathematical derivation is under review [14]. In the current work, we test the recently-derived approximations numerically in a variety of situations of relevance to atomic and molecular systems. We show that, even when TF theory is surprisingly accurate for quantities integrated over the entire system (such as the total energy or its components), the uniform semiclassical approximations capture the leading-corrections within a given region of space. We use the pointwise formulas to derive analytic corrections to the TF energies, and confirm these numerically on a class of potentials. But we also find that many such contributions cancel *exactly* between classically-allowed and forbidden regions, which leads to high accuracy of TF theory for integrated quantities, despite poor pointwise behavior.

To illustrate the main ideas of this paper, in Fig. 1 we plot a sequence of densities for same-spin fermions in a harmonic well, $v(x) = x^2/2$. In each curve, we replace \hbar by $\gamma\hbar$, N by N/γ , and $n(x)$ by $\gamma n(x)$, where γ is made successively smaller. In the limit $\gamma \rightarrow 0$, the exact quantum curve weakly approaches the TF density. The uniform semiclassical approximation is so accurate as to be indistinguishable from the exact curves here, even for $N = 1$, although it only includes the leading corrections to TF as $\gamma \rightarrow 0$. By any *pointwise* measure, it is vastly

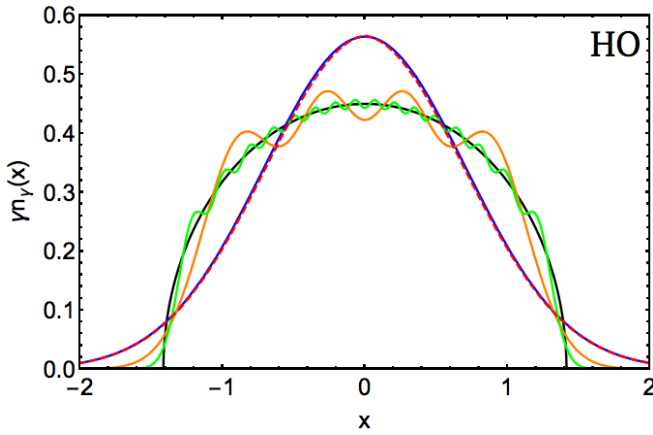


FIG. 1. $\gamma n_\gamma(x)$ for $N = 1$ harmonic potential where $\gamma = 1$ (blue, with semiclassical approximation dashed red), $1/4$ (orange), $1/16$ (green), and TF (black).

superior to TF. Results within this paper demonstrate this for several different potentials.

But DFT cares almost solely about energies [19]. To connect the pointwise success of the uniform approximation with these, we calculate the integrated densities and energy-densities in forbidden and allowed regions separately. The semiclassical approximations allow us to derive leading corrections to TF in each region analytically, and check the results numerically. These are universal formulas that apply to all (non-pathological) 1D potentials. Again, the uniform approximations are vastly superior to TF theory. However, we also show that the improvements in allowed and forbidden regions are always equal and opposite, and so *cancel* from the total energy components. The harmonic oscillator is a stark example: because TF theory yields the exact energy components for this case, the semiclassical approximation always *worsen* those energies!

This paper is devoted to demonstrating these facts and discussing their consequences. We review in Section II A the semiclassical limit of nonrelativistic fermionic systems. In Sec. II B we establish the adopted notation while providing a brief discussion of the uniform semiclassical approximations derived in Refs. [13, 14]. Sec. III is devoted to describing both numerical and analytic calculations. Section IV provides a detailed description of the leading corrections to TF components in different regions of configuration space, ranging from pointwise (Sec. IV A) to regional (Sec. IV B) and finally global (Sec. IV C). In Sec. V, we study situations that differ qualitatively from the generic wells studied up to that point. We see the breakdown of the semiclassical approximation when the potential varies too rapidly (Sec. V A), how extended systems can be treated (Sec. V B) and tunneling in a double well (Sec. V C). We close with a discussion of the significance of these results, especially in the context of density functional theory. The appendix collects useful results about the Airy functions used in this paper.

II. BACKGROUND

A. General semiclassical limit of nonrelativistic fermionic systems

Lieb and Simon proved in 1973 [5] that quantum-mechanical nonrelativistic fermionic systems interacting via the Coulomb interaction are exactly described by TF theory in the semiclassical limit. In particular, this implies the relative error of expectation values predicted by TF theory goes to zero as the nuclear charges Z in the system go to infinity. The reason Z gets involved here is that it sets the relevant length scales for the Coulombic problem [20].

More recently, Fournais et al. [21] proved that a generalization of the Lieb-Simon result is valid in any number of spatial dimensions, i.e., under semiclassical scaling, all correlation functions of a quantum-mechanical system (and therefore, all of its properties) agree with those obtained by minimization of the TF energy functional in a well-defined limit. Specifically, the predictions of TF theory emerge from quantum mechanics when the number of particles N is scaled to infinity and $\hbar \rightarrow 0$ as $N^{-1/d}$, where d is the dimensionality of the considered configuration space. Hereafter, we restrict considerations to 1D.

B. Relevant classical variables and Thomas-Fermi theory

Consider a 1D Hamiltonian

$$\hat{h} = -\frac{1}{2} \frac{d^2}{dx^2} + v(x). \quad (1)$$

We consider potentials that either vanish or diverge positively at large $|x|$. In the former case, we require at least one bound state for the employed methods to be relevant. We are interested in the ground-state of N noninteracting same-spin fermions at 0K in this potential. We list the eigenvalues in increasing order, ϵ_j , $j = 1, 2, \dots, N$. Then we may write the particle density as

$$n(x) = \sum_{j=1}^N |\phi_j(x)|^2, \quad \int_{-\infty}^{\infty} dx n(x) = N. \quad (2)$$

The kinetic energy may be written many ways, but we chose a specific kinetic-energy density,

$$\begin{aligned} t(x) &= \sum_{j=1}^N [\epsilon_j - v(x)] |\phi_j(x)|^2, \quad \int_{-\infty}^{\infty} dx t(x) = T. \\ &= -\frac{1}{2} \sum_{j=1}^N \phi_j^*(x) \frac{d^2 \phi_j(x)}{dx^2}. \end{aligned} \quad (3)$$

Unlike the particle density, the choice of kinetic energy density is arbitrary, as the kinetic energy density is not a physical observable.

Our focus is semiclassical approximations, which require classical inputs. For a given energy ϵ , we consider only the case of two turning points (denoted $x_L(\epsilon)$ and $x_R(\epsilon)$) at which the classical momentum

$$k(\epsilon, x) = \sqrt{2[\epsilon - v(x)]}, \quad (4)$$

vanishes. We define the corresponding classical phase and time for the particle to arrive at x , starting from $x_L(\epsilon)$, as:

$$\begin{aligned} \theta(\epsilon, x) &= \int_{x_L(\epsilon)}^x dx' k(\epsilon, x'), \\ \tau(\epsilon, x) &= \int_{x_L(\epsilon)}^x \frac{dx'}{k(\epsilon, x')}. \end{aligned} \quad (5)$$

The classical action for energy ϵ is determined by the total phase from left to right turning points:

$$I(\epsilon) = \frac{\theta_L[\epsilon, x_R(\epsilon)]}{\pi}. \quad (6)$$

Inversion yields the energy as a function of the action, $\epsilon(I)$, and the frequency corresponding to the motion is

$$\omega(\epsilon) = \frac{\pi}{T(\epsilon)} = \frac{d\epsilon}{dI}, \quad (7)$$

where $T(\epsilon) = \tau[\epsilon, x_R(\epsilon)]$. The corresponding angle variable is then

$$\alpha(\epsilon, x) = \omega(\epsilon)\tau(\epsilon, x). \quad (8)$$

All of the classical observables given above can be obtained from the classical phase $\theta(\epsilon, x)$ by application of partial derivatives. For instance,

$$\begin{aligned} k(\epsilon, x) &= \frac{\partial \theta(\epsilon, x)}{\partial x}, \quad \tau(\epsilon, x) = \frac{\partial \theta(\epsilon, x)}{\partial \epsilon}, \\ \alpha(\epsilon, x) &= \frac{\partial \theta(\epsilon, x)}{\partial I}, \quad T(\epsilon) = \frac{\partial \theta(\epsilon, x_R)}{\partial \epsilon}. \end{aligned} \quad (9)$$

The WKB quantization condition for the energy of the j -th level is

$$I(\epsilon_j^{\text{WKB}}) = \hbar \left(j - \frac{1}{2} \right). \quad (10)$$

We define the semiclassical Fermi energy for N particles by

$$\epsilon_F = \epsilon_{N+1/2}^{\text{WKB}}, \quad (11)$$

i.e., we set the quantum number j midway between the index of the highest occupied level and lowest unoccupied one, and use a subscript F to denote quantities evaluated at this energy. We can also define the mid-phase point x_m at which

$$\theta_F(x_m) = N\pi/2. \quad (12)$$

At the Fermi energy, we adopt the convention of always measuring classical variables from their nearest turning point as measured by the classical phase. This leads to small kinks in $\theta_F(x)$ and $\alpha_F(x)$ as x goes through x_m but which become irrelevant in the semiclassical limit (see Eq. 36 of Ref. [14]). For potentials that are symmetric about $x = 0$, it follows that $x_m = 0$. Since one can always treat a right-hand turning point by applying left-hand formulas to $v(-x)$, we here give only formulas for $x < x_m$.

In 1D it is particularly easy to explicitly connect TF theory with semiclassical approximations. In the limit where $\hbar \rightarrow 0$, the WKB energy for a system with N occupied orbitals is simply the sum of all occupied semiclassical orbital energies. On the other hand, by approximating the discrete sum of WKB orbital densities as an integral and ignoring quantum oscillations and exponentially small terms, then it follows that

$$n(x) = \frac{k_F(x)}{\pi}, \quad t(x) = \frac{k_F^3(x)}{6\pi} \quad (\text{PFT}), \quad (13)$$

where PFT denotes potential functional theory, i.e., both quantities are given as functionals of the potential. Elimination of $k_F(x)$ yields the TF expression for the 1d kinetic energy density functional:

$$t(n) = \frac{\pi^2 n^3}{6}. \quad (\text{DFT}) \quad (14)$$

To study the semiclassical limit of noninteracting 1d fermions [21] we define positive real-valued parameters γ , scaled particle number N_γ , and scaled Planck's constant \hbar_γ , where,

$$N_\gamma = \frac{N}{\gamma}, \quad \hbar_\gamma = \gamma \hbar. \quad (15)$$

The semiclassical limit arises when $\gamma \rightarrow 0$. This has been extensively discussed in Refs [7, 10, 14, 21]. For instance, in Ref. [10], Cangi et al. derived semiclassical approximations for the particle and kinetic energy densities of systems with closed (box) boundary conditions with the requirement that they provide the leading corrections to TF theory when γ is sufficiently small. Recently, we generalized the approach of Ref. [10] to the case of unbounded domains [13, 14]. In Ref. [13] we provided a sketch of the construction of the semiclassical approximations, whereas Ref. [14] explored the mathematical intricacies of such construction.

Under γ -scaling the TF densities change trivially:

$$n_\gamma^{\text{TF}}(x) = \frac{k_F(x)}{\pi\gamma}, \quad t_\gamma^{\text{TF}}(x) = \frac{k_F^3(x)}{6\pi\gamma}, \quad (16)$$

Thus both energy components (kinetic and potential) scale as γ^{-1} .

While it is easy to find the dominant behavior of any observable in the limit where $\gamma = 0$, i.e., via TF theory, it took about 50 years to find a general universally valid result for the leading corrections [13, 14]. The behavior and accuracy of these expressions are relatively

unexplored. We also note that there is no general procedure for finding the leading corrections to the TF density functionals of Eq. (14). The semiclassical expressions are all functionals of the potential [12, 13, 22]

Going beyond the dominant contribution also means including evanescent behavior. All of the spatially-varying quantities presented above have a clear classical meanings for $x_L(\epsilon) \leq x$. However, they become purely imaginary in a region which is classically-forbidden. We define

$$-ik(\epsilon, x) = \sqrt{2[v(x) - \epsilon]}, \quad x < x_L(\epsilon), \quad (17)$$

which ensures that $-i\theta$, $-i\tau$ and $-i\alpha$ are real for all $x < x_L$. With these definitions, all of the previously identified classical quantities are extended to any $x \in x < x_L$.

C. Uniform semiclassical approximations

The Langer wave function is a uniform semiclassical generalization of the WKB results that remains finite as one passes through a turning point, and is expressed in terms of Airy functions[18]. By taking the semiclassical limit of finite sums of the squares of such functions, the main results of Ref. [13] are obtained[14]. We write these here in a simple form

$$\begin{aligned} n^{sc}(x) &= f_1^{sc}[k_F(x), d_F(x), \theta_F(x)], \\ t^{sc}(x) &= \frac{k_F^2}{6} f_3^{sc}[k_F(x), d_F(x), \theta_F(x)], \end{aligned} \quad (18)$$

where

$$d_F(x) = k_F(x) \sin \alpha_F(x) / \omega_F, \quad (19)$$

and

$$f_p^{sc}(k, d, \theta) = \frac{1}{\pi} \left(k K_0(\theta) + p \frac{K_1(\theta)}{d} \right), \quad (20)$$

with K_j being known combinations of products of Airy functions given in Appendix A, and $d_F(x)$ is a classical measure of distance. The input classical variables are plotted in Fig. 2 for a simple harmonic oscillator, with the origin at the Fermi turning point, and using the above convention for the evanescent region. We see that these quantities are all comparable in magnitude and approach the turning point in diverse ways.

The mathematical underpinnings of the above have been discussed in detail in Ref. [14]. Here we just recall that the analytical continuations given before for the spatially-varying classical quantities ensure that the particle density is continuous and real everywhere in configuration space. It also positive everywhere except in pathological situations where $v'(x_F) \rightarrow 0$, where x_F is the Fermi turning point. While the above supposes that $v(x)$ consists of a single potential well, we also discuss the generalization to the case of weakly-coupled multiple wells in Sec V C below.

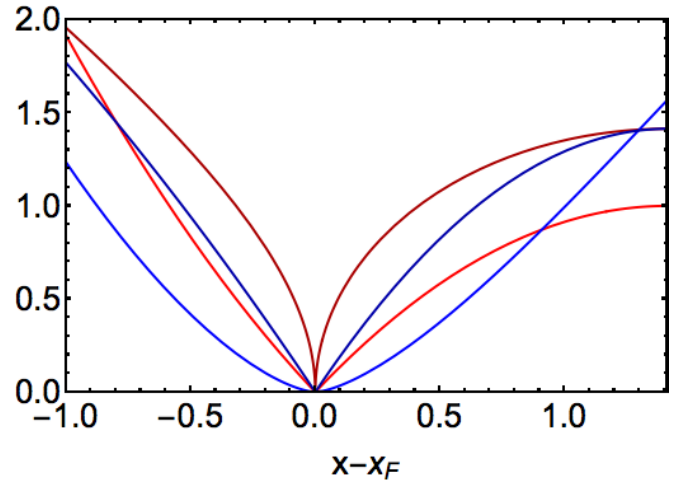


FIG. 2. Classical properties of ϵ_F trajectory for the SHO with $N = 1$ vs. $x - x_F$. Red is $\epsilon_F - v(x)$, dark red is $k_F(x)$, blue is $\theta_F(x)$, and dark blue is $d_F(x)$.

In the derivation of Eq. (20), the first part comes from the 0th-order term in the Poisson summation formula, while the second is the dominant correction from the oscillating pieces [13, 14]. If K_1 is set to zero a first approximation to the density is obtained, though it is in general uncontrollable.

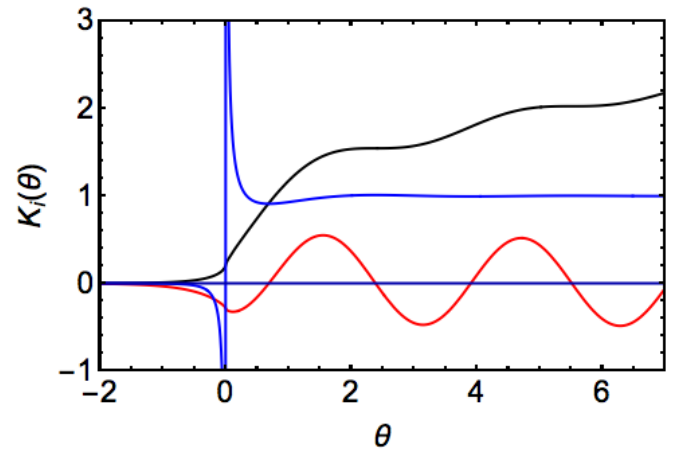


FIG. 3. K_i functions versus θ , with K_i versus $-i\theta$ in evanescent region. K_0 is blue, K_1 is red, and K_2 is black.

In Fig. 3, we plot the K_j functions against θ , adopting the convention mentioned above for the evanescent region. They contain both the quantum oscillations of the travelling region ($\theta \gg \pi$), the singular behavior near the turning point ($\theta \sim 0$), and the evanescent behavior far from the turning point ($-i\theta \ll 0$). In the region of the turning point, the different power-law behaviors of the classical variables balance the singular to produce continuous and largely smooth behavior in Eq. (20). On a large scale, $K_0 \approx H(\theta)$ and $K_1 = 0$, where H is the Heaviside step function. Inserted in Eq. 18, this yields

the TF results. The function K_2 is useful in Sec IV B where we explore the small γ limit.

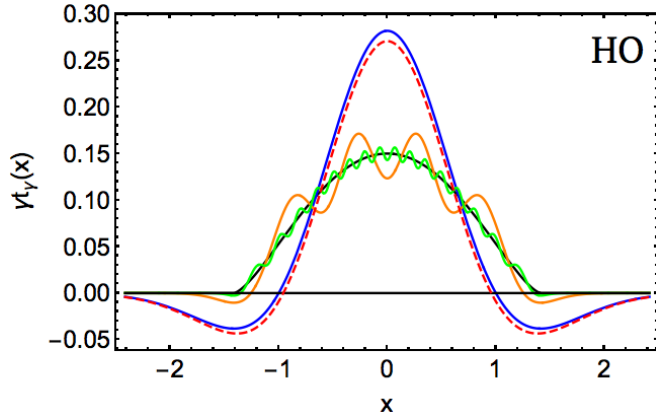


FIG. 4. Same as Fig. 1, but for the kinetic energy density.

The value of this representation becomes clear when we reintroduce γ . Then

$$\left\{ \begin{array}{l} n_{\gamma}^{sc}(x) \\ t_{\gamma}^{sc}(x) \end{array} \right\} = \frac{f_p^{sc}(k_F(x), d_F(x), \theta_F(x)/\gamma)}{\gamma}, \quad (21)$$

i.e., beyond the trivial scaling with γ , only the phase argument depends on γ , as all other quantities are purely classical. As $\gamma \rightarrow 0$, only the arguments of the K_i functions change, becoming much larger for any fixed x . Alternatively, the region of $|\theta| < \xi$, for fixed ξ , which we call the turning-point region, shrinks to a region in x space of size γ .

In Fig. 1 we only show the result given by the semiclassical formula for $\gamma = 1$. For all other values of γ , the semiclassical formula is everywhere indistinguishable from the exact curve. In Fig. 4, we plot the analogous curve for the scaled kinetic energy density, for which the semiclassical approximation is (slightly) less accurate.

In Fig. 5, we plot the ratio of semiclassical and exact densities for different values of γ . It appears to approach 1 everywhere, showing that its relative error vanishes for sufficiently small γ , for all values of x . This shows that it is a *uniform* asymptotic expansion and suffers none of the difficulties of patching for different regions, despite the qualitatively different behavior of spatially-varying properties in the traveling, transition and evanescent regions. In fact, for $|x|$ sufficiently large, the semiclassical density decay is exponential in $|\theta_F(x)|$ (see Eq. (22) of Ref. [13]), which does not match the decay of the exact density, which is dominated by the highest occupied level, $|\phi_N(x)|^2$. Thus the fractional error eventually grows again beyond the edges of the figure. But as $\gamma \rightarrow 0$, the point at which this error becomes noticeable becomes ever larger.

These formulas are remarkable for their ability to yield extremely accurate results using *only* classical inputs. Fig. 1 shows that, for the ground-state of the harmonic oscillator, they yield densities that are indistinguishable

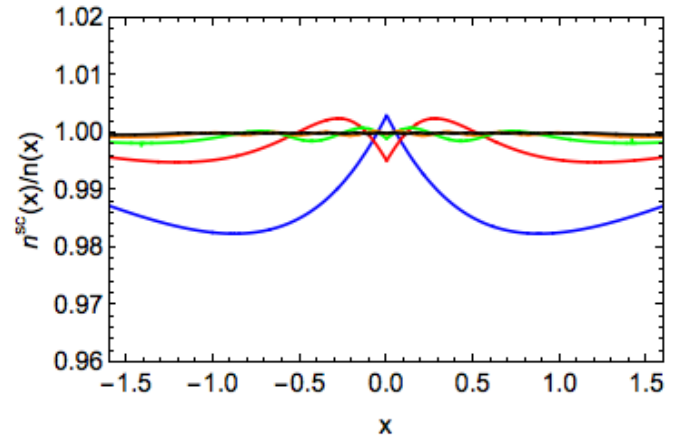


FIG. 5. $n^{sc}(x)/n(x)$ for the harmonic oscillator with $\gamma = 1$ (blue), $1/2$ (red), $1/4$ (green), $1/8$ (orange), and $1/16$ (black).

from the exact quantum curves. Yet no differential equation has been solved to evaluate them, and they apply to all potentials. The smoother the potential is, the more accurate the result will be, even with only one occupied level.

III. METHODS

A. Numerical

One of the great features of the uniform semiclassical approximations for the particle and kinetic energy densities is that they allow us to obtain these quantities with minimal effort. This is to the contrary of numerically solving the Schrodinger equation for systems with a large number of particles. In this section we explain the numerical methods employed in the paper to compare semiclassical and Thomas-Fermi theory with exact results.

Accurate numerical solutions for the Schrodinger equation were extracted with the Matrix Numerov method [23] whenever the studied potential could not be solved analytically. A grid spacing of $O(10^{-3})$ was chosen and the size L of the studied region depended on each potential. This choice of parameters was guided by the requirement that both kinetic and total energies converge (relative to both grid spacing and L) up to at least the 3rd decimal digit (except for the double wells where we only enforced convergence up to the 2nd decimal digit). In every case we checked that both the exact particle and kinetic energy densities were at least of $O(10^{-5})$ when $x = \pm L$. For calculations with $\gamma \ll 1$, smaller grid spacings were needed to capture the oscillations and the more rapid decay in the evanescent region. Mathematica 10.1 was employed in all computations [24].

B. Analytical

Several potentials are employed to illustrate our results. Most have analytic forms for at least their semiclassical quantities, and many have exact solutions. All are infinitely differentiable. These are illustrated in Fig. 6. For each form, we calculate both standard semiclassical quantities, and all the derived quantities used in this paper. We also give the TF results. These are collected in Table I.

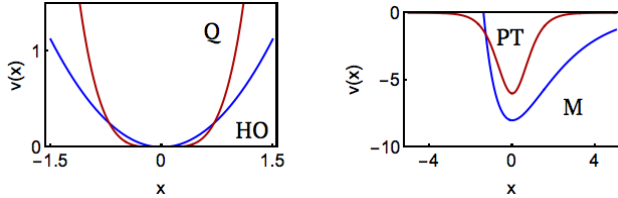


FIG. 6. Analytic potentials employed for the systematic investigation of the uniform semiclassical approximations.

For any potential, the WKB energy components of each individual level can be immediately extracted if $\epsilon_j^{sc}[\beta v(x)]$ is known, where $\beta > 0$. Then

$$v_j = \left. \frac{\partial \epsilon_j}{\partial \beta} \right|_{\beta=1} \quad (22)$$

is the potential contribution, and t_j may be found by subtraction. As indicated by March and Plaskett[25], TF energies may be found by applying the Poisson summation formula to evaluate the corresponding sum of WKB energy components over occupied orbitals, and retaining only the average contribution, e.g.,

$$T^{\text{TF}} = \int_{-\frac{1}{2}}^{N-\frac{1}{2}} dj t_j^{sc} \quad (23)$$

with similar forms for the other components. Because simple explicit results for WKB energies are known for many potentials, the above allows a quick generation of TF energy components.

In those cases where analytic expressions are available for the exact energy components, one can extract the γ -dependence of an energy component as:

$$T_\gamma(N, D, a) = T(N/\gamma, a/\gamma, D), \quad (24)$$

where D is the well-depth, and $1/a$ is a characteristic length scale (see Table I). By taking $\gamma \rightarrow 0$, the dominant term is given by TF, and we denote the next correction as $T^{(1)}$, e.g.,

$$T_\gamma \rightarrow T^{\text{TF}}/\gamma + \gamma T^{(1)} + \dots \quad (25)$$

This is also listed Table I. Table III gives numerical values for the constants associated to each potential we studied in this paper.

IV. LEADING CORRECTIONS TO THOMAS-FERMI ENERGIES

A. Pointwise accuracy

Figures 1, 4 and 5 demonstrate the much greater accuracy of the semiclassical approximations relative to those of TF, *pointwise* in space. For many applications, this is terribly important, such as e.g., in the calculation of a surface energy. However, in the world of DFT, there is overwhelming importance given to knowing energies as functionals of the density. So, while the semiclassical formulas yield great improvements over the local approximation pointwise, what is their performance for energies (which depend on global averages)? Answering the above question is one of the main purposes of the present paper, and we show below the answer is more complicated than expected.

We begin to illustrate the issue by using the density- and kinetic energy-error measures introduced in Ref. [13], which are given by:

$$\begin{aligned} \eta &= \frac{1}{N} \int_{-\infty}^{\infty} dx |\tilde{n}(x) - n(x)|, \\ \zeta &= \frac{1}{T} \int_{-\infty}^{\infty} dx |\tilde{t}(x) - t(x)|, \end{aligned} \quad (26)$$

where \tilde{n} (\tilde{t}) indicates an approximate density (kinetic energy density), and T is the exact kinetic energy. The density-error measure is chosen so that it does not vanish too rapidly with increasing accuracy of the approximation, and is normalized to 2 if the approximate density has no overlap with the exact one. Table II shows these errors for a harmonic oscillator with unit frequency as a function of γ for both the particle- and the kinetic-energy densities as given by both TF and semiclassical theories. Even for $\gamma = 1$, the semiclassical density error is almost two orders of magnitude smaller than that of TF, and vanishes much more rapidly with decreasing γ . The improvement in the kinetic energy density error is still very good (the semiclassical error vanishes as $\gamma \rightarrow 0$, while TF does not), though not as spectacular at $\gamma = 1$.

Another beautiful illustration of the semiclassical formulas is seen by considering the particle- and kinetic-energy densities at the turning point of the semiclassical Fermi energy. The explicit formulas are derived by expanding Eq. (18) around a turning point. This yields [13, 14, 26]

$$l_F n_\gamma^{sc}(x_F) \rightarrow \frac{c_0}{\gamma^{2/3}} - c_1 b_F, \quad l_F^3 t_\gamma^{sc}(x_F) \rightarrow -\frac{c_1}{6}, \quad (27)$$

where

$$l_F = (2|v'_F|)^{-1/3}, \quad (28)$$

$c_0 = (12\pi^2 a_0^2)^{-1}$, $c_1 = (2\pi\sqrt{3})^{-1}$, and

$$b_F = \frac{1}{3} \left(\phi_F^2 + \frac{4\chi_F}{5} \right), \quad (29)$$

	harmonic	quartic	Poschl-Teller	Morse
$v(x)$	$x^2/2$	x^4	$-D/\cosh^2(ax)$	$D[(1 - e^{-ax})^2 - 1]$
ϵ_j	\tilde{j}	—	$-a^2(\alpha_e - \tilde{j})^2/2$	$-a^2(\alpha - \tilde{j})^2/2$
ϵ_j^{sc}	ϵ_j	$(d_4 \tilde{j})^{4/3}$	$-a^2(\alpha - \tilde{j})^2/2$	ϵ_j
t_j	$\tilde{j}/2$	—	$a^2(\alpha^2/\alpha_e - \alpha_e + \tilde{j})(\alpha_e - \tilde{j})/2$	$a^2 \tilde{j}(\alpha - \tilde{j})/2$
t_j^{sc}	t_j	$2(d_4 \tilde{j})^{4/3}/3$	$a^2 \tilde{j}(\alpha - \tilde{j})/2$	t_j
v_j	$\tilde{j}/2$	—	$-D(1 - \tilde{j}/\alpha_e)$	$-D(1 - \tilde{j}/\alpha)$
v_j^{sc}	v_j	$t_j^{sc}/2$	$-D(1 - \tilde{j}/\alpha)$	v_j
Classical energy variables				
$\omega(\epsilon)$	1	$4d_4^{1/3} \epsilon^{1/4}/3$	$a\sqrt{-2\epsilon}$	$a\sqrt{-2\epsilon}$
$I(\epsilon)$	ϵ	$\epsilon^{3/4}/d_4$	$\alpha - \sqrt{-2\epsilon}/a$	$\alpha - \sqrt{-2\epsilon}/a$
Fermi level				
ϵ_F	N	$(d_4 N)^{4/3}$	$-(\alpha\alpha\beta)^2/2$	$-(\alpha\alpha\beta)^2/2$
ω_F	1	$4d_4^{1/3} N^{1/3}/3$	$a^2\alpha\beta$	$a^2\alpha\beta$
x_F	$-\sqrt{2N}$	$-d_4^{1/3} N^{1/3}$	$-\cosh^{-1}(1/\beta)/a$	$-\log(1 \pm \bar{\beta})/a$
l_F	$2^{-1/2} N^{-1/6}$	$(d_4 N)^{-1/3}/2$	$(2\alpha^2\beta^2\bar{\beta})^{-1/3}/a$	$(2\alpha^2\bar{\beta})^{-1/3}(1 \pm \bar{\beta})^{-1/3}/a$
v_F''	1	$12(d_4 N)^{2/3}$	$\alpha^2 a^4 \beta^2 (\beta^2 - 2\bar{\beta}^2)$	$\alpha^2 a^4 (3 \pm 3\bar{\beta} - 2\beta^2)$
Dimensionless parameters				
ϕ_F	$N^{-2/3}/2$	$d_4^{2/3} N^{-1/3}/3$	$(4\alpha\bar{\beta}^2)^{-1/3}$	$(4\alpha\bar{\beta}^2)^{-1/3}(1 \pm \bar{\beta})^{-2/3}\beta$
χ_F	$N^{-2/3}/4$	$3(d_4 N)^{-2/3}/4$	$(16\alpha^2\beta^2\bar{\beta}^4)^{-1/3}(\beta^2 - 2\bar{\beta}^2)$	$\alpha^{-2/3}[2(\bar{\beta} \pm \bar{\beta}^2)]^{-4/3}(3 - 2\beta^2 \pm 3\bar{\beta})$
$l_F^2 \epsilon_F$	$N^{2/3}/2$	$(d_4 N)^{2/3}/4$	$-(\alpha^2\beta^2\bar{\beta}^{-2}/4)^{1/3}/2$	$-(\bar{\beta} \pm \bar{\beta}^2)^{-2/3}\alpha^{2/3}\beta^2/2$
b_F	$9N^{-2/3}/60$	$d_5 (d_4 N)^{-2/3}$	$2(\alpha^2\beta^2\bar{\beta}^4)^{-1/3}(5 + 4\beta^2 - 8\bar{\beta}^2)/30$	$\frac{5\beta^2 + 4(3 - 2\beta^2 \pm 3\bar{\beta})}{30(\sqrt{2}\alpha)^{2/3}(\bar{\beta} \pm \bar{\beta}^2)^{4/3}}$
Total energies				
T	$N^2/4$	—	$a^2 N[-N^2/3 + N(\alpha_e - \alpha^2(2\alpha_e)^{-1}) - 1/6]/2$	$a^2 N(-N^2/3 + \alpha N/2 + 1/12)/2$
T^{TF}	T	$2d_4^{1/3} N^{7/3}/7$	$a^2 N(-N^2/3 + \alpha N/2)/2$	$a^2 N(-N^2/3 + \alpha N/2)/2$
$T^{(1)}$	0	—	$a^2 N[9N(8\alpha)^{-1} - 1]/12$	$a^2 N/24$
V	T	—	$-\alpha^2 a^2 N[-N(2\alpha_e)^{-1} + 1]/2$	$-a^2 \alpha N(-N + 2\alpha)/4$
V^{TF}	T	$T^{TF}/2$	$-a^2 \alpha N(-N + 2\alpha)/4$	V
$V^{(1)}$	0	—	$-a^2 N^2(32\alpha)^{-1}$	0
E	$2T$	—	$-a^2 N(N^2/3 - \alpha_e N + \alpha^2 + 1/6)/2$	$-a^2 N(N^2/3 - \alpha N + \alpha^2 - 1/12)/2$
E^{TF}	E	$3T^{TF}/2$	$-a^2 N(N^2/3 - \alpha N + \alpha^2)/2$	$-a^2 N(N^2/3 - \alpha N + \alpha^2)/2$
$E^{(1)}$	0	—	$a^2 N[3N(4\alpha)^{-1} - 1]/12$	$a^2 N/24$

TABLE I. Potentials and useful formulas, both exact and semiclassical. Notation: $\tilde{j} = j - 1/2$, $d_4 = 3\pi^{3/2}\Gamma^{-2}(1/4) \approx 1.270820$, $d_5 = 1/5 + d_4^2/27 \approx 0.259814$, $\alpha = \sqrt{2D/a^2}$, $\alpha_e = \sqrt{2D/a^2 + 1/4}$, $\beta = 1 - \alpha N$, $\bar{\beta} = \sqrt{1 - \beta^2}$. Dashes indicate no analytical result.

γ	η^{sc}	η^{TF}	ζ^{sc}	ζ^{TF}
1	0.0118	0.2552	0.1284	0.8445
1/2	0.0026	0.1558	0.0320	0.4164
1/4	0.0007	0.0913	0.0082	0.2063

TABLE II. Semiclassical and TF pointwise errors for the particle and kinetic energy densities of the SHO ($N = 1$)

with

$$\phi_F = l_F^2 \omega_F, \quad \chi_F = l_F^4 v_F''.$$

The length scale l_F is that used by Kohn and Mattson[27] to characterize the Airy gas. It is the length scale defined by the gradient of the potential at a turning point defined by the Fermi energy, and determines the $\gamma \rightarrow 0$ behavior of both particle and kinetic densities at the turning point. On the other hand, the leading correction to the turning-point density contains two other scales: ω_F , the classical

frequency of a trajectory at the Fermi energy, and v_F'' , the second derivative of the potential at the turning point. These can both be given in dimensionless quantities using l_F . Thus χ_F is a dimensionless measure of the second derivative of the potential and is a locally-determined quantity (apart from the energy at which it is evaluated), while ϕ_F is mixed, as it includes ω_F , a global property, evaluated on the local length scale, l_F .

In Figs 7 and 8, we plot $n_\gamma^{sc}(x_F)$ and $t_\gamma^{sc}(x_F)$ for the harmonic oscillator and both sides of the Morse potential (with $N = 1$). A universal limit is clearly shown by Fig. 7 which was first identified by Kohn and Sham[26]. However, it also shows that the next correction obtained with the semiclassical uniform approximation is appropriate, and that these two terms alone yield results at $\gamma = 1$ that are accurate to within 2%. Table III indicates the Morse potential produces values of b_F for the left and right turning points which are very close and only slightly larger than those of the HO. Hence the bunching of the

	SHO	Q	PT	Morse	PT (δ)	PT (δ)	Double Well	
$v(x)$	$x^2/2$	x^4	$D = 21, a = 1$	$D = 8, a = 1/2$	$\delta = 1/8$	$\delta = 1/64$	$b = 3.0$	$b = 3.3$
ϵ	0.500	0.668	-18.000	-7.031	-0.262	-0.200	1.29, 1.43	1.52, 1.56
ϵ^{sc}	0.500	0.546	-17.884	-7.031	-0.191	-0.133	1.41	1.57
t	0.250	0.445	1.385	0.469	0.107	0.088	0.76, 1.21	0.77, 0.63
t^{WKB}	0.250	0.364	1.495	0.469	0.154	0.129	NC	NC
v	0.250	0.223	-19.384	-7.500	-0.370	-0.288	0.66, 0.84	0.79, 0.88
v^{WKB}	0.250	0.182	-19.380	-7.500	-0.345	-0.262	NC	NC
Fermi level								
ϵ_F	1.000	1.376	-15.019	-6.125	-0.007	-0.0001	2.51	2.96
ω_F	1.000	1.835	5.481	1.750	0.118	0.0155	1.45	2.50
x_F	-1.414	-1.083	-0.595	-0.789, -1.323	-2.939	-4.875	-2.120, -0.087	-2.270, -0.539
l_F	0.707	0.462	0.315	0.443, 0.630	3.305	12.765	0.375, 1.088	0.356, 0.576
v_F''	1.000	14.079	4.373	11.684, 0.065	-0.027	-0.0005	22.455, -4.455	25.482, -3.702
Dimensionless parameters								
ϕ_F	0.500	0.391	0.543	0.343, 0.695	1.289	2.526	0.204, 1.712	0.318, 0.829
χ_F	0.250	0.639	0.043	0.450, 0.010	-3.268	-12.762	0.443, -6.241	0.411, -0.406
$l_F^2 \epsilon_F$	0.500	0.293	-1.488	-1.202, -2.432	-0.076	-0.020	0.353, 2.976	0.376, 0.980
b_F	0.150	0.221	0.110	0.159, 0.164	-0.442	-1.275	0.186, -1.091	0.216, 0.168
Regional energies								
T^{allow}	0.293	0.519	1.618	0.547	0.113	0.089	1.37	1.65
$T^{\text{allow,TF}}$	0.250	0.393	1.453	0.458	0.113	0.087	1.15	1.41
$T^{\text{allow,sc}}$	0.266	0.401	1.542	0.484	0.113	0.084	1.22	1.50
T^{forbid}	-0.043	-0.074	-0.233	-0.078	0.000	0.000	-0.33	-0.24
$T^{\text{forbid,TF}}$	0.000	0.000	0.000	0.000	0.000	0.000	0.00	0.00
$T^{\text{forbid,sc}}$	-0.047	-0.118	-0.220	-0.090	0.000	0.000	-0.01	-0.25
V^{allow}	0.185	0.123	-18.791	-7.621	-0.370	-0.305	1.27	1.29
$V^{\text{allow,TF}}$	0.250	0.197	-19.380	-7.500	-0.345	-0.262	1.56	1.67
$V^{\text{allow,sc}}$	0.182	0.122	-18.596	-7.627	-0.335	0.249	1.30	1.27
V^{forbid}	0.065	0.093	-0.593	-8.009	0.000	0.000	0.29	0.38
$V^{\text{forbid,TF}}$	0.000	0.000	0.000	0.000	0.000	0.000	0.00	0.00
$V^{\text{forbid,sc}}$	0.065	0.099	-0.622	-8.009	0.000	0.000	0.21	0.37
Total energies								
T	0.250	0.445	1.385	0.469	0.107	0.088	1.21	1.41
T^{TF}	0.250	0.393	1.453	0.458	0.113	0.087	1.15	1.41
T^{sc}	0.218	0.283	1.322	0.419	0.112	0.084	1.04	1.25
$T^{(1)}$	0.000	NA	-0.069	0.010	0.0005	-0.055	NC	NC
V	0.250	0.223	-19.384	-7.500	-0.370	-0.288	1.51	1.67
V^{TF}	0.250	0.197	-19.380	-7.500	-0.345	-0.262	1.56	1.67
V^{sc}	0.246	0.222	-19.219	-7.508	-0.335	-0.249	1.56	1.64
$V^{(1)}$	0.000	NA	-0.005	0.000	-0.028	-0.031	NC	NC
E	0.500	0.668	-18.000	-7.031	-0.262	-0.200	2.72	3.08
E^{TF}	0.500	0.590	-17.926	-7.042	-0.232	-0.175	2.71	3.08
E^{sc}	0.464	0.505	-17.897	-7.089	-0.223	-0.165	2.60	2.89
$E^{(1)}$	0.000	NA	-0.074	0.010	-0.027	-0.086	NC	NC

TABLE III. Numerical values of parameters for each potential used in this paper, with $N = 1$ in each. When two values appear, they correspond to left- and right-turning points respectively. NC denotes not calculated.

straight lines in Fig. 7.

Our result, Eq. (27), for the kinetic-energy turning-point density, is likewise universal, but does not produce the correct leading correction. The derivation of Ref. [14] guarantees only that the leading terms should be correct, and our figures are numerical illustrations of this fact. It is an added bonus that the leading correction is also appropriate for the density. That it is not so for the kinetic energy density reflects the greater difficulty in achieving the same number of terms in the expansion

in γ for the kinetic energy, because of the two spatial derivatives in the operator.

B. Regional particle numbers and energies

The previous subsection demonstrates the far greater accuracy of the uniform approximation relative to TF, both at every point in space, and at a special one, the Fermi turning point. But this is a measure-zero set, so

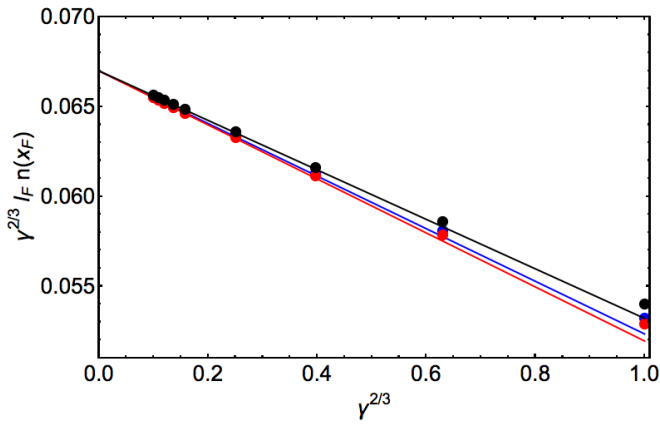


FIG. 7. Scaled dimensionless turning-point density, $\gamma^{2/3} l_F n(x_F)$, as a function of γ for several potentials. Points are exact, straight lines are the leading behavior of the semiclassical formula, Eq. 21. Black is harmonic oscillator, and blue and red are the left and right turning points of a Morse potential of depth 6 ($a = 1$).

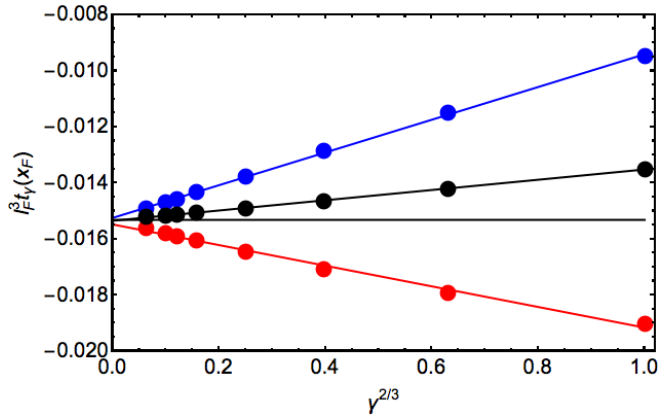


FIG. 8. Same as Fig. 7, but for the scaled dimensionless kinetic energy turning-point density, $l_F^3 t_\gamma(x_F)$.

that comparisons such as the one just shown do not imply much about the accuracy of expectation values over the entire system. So next, as we do throughout this section, we separate errors in the traveling region from those in the evanescent region. We write

$$f^{\text{allow}} = \int_{x_F}^{x_m} dx f(x), \quad f^{\text{forbid}} = \int_{-\infty}^{x_F} dx f(x), \quad (31)$$

so that

$$\int_{-\infty}^{\infty} dx f(x) = f^{\text{forbid,L}} + f^{\text{allow,L}} + f^{\text{allow,R}} + f^{\text{forbid,R}} \quad (32)$$

where the superscripts denote the left and right contributions, respectively. This is a basic method of capturing some fraction of real-space information, while being able to connect to global integrals trivially. Most importantly, it allows integration over the detailed quantum oscillations introduced by the semiclassical approximation.

The behavior of the semiclassical expansion is very different in the neighborhood of a turning point than either in the interior allowed region or exterior forbidden. To analyze it, we note that, as $\gamma \rightarrow 0^+$, the potential in the region where $|\theta|/\gamma < \xi$, with $\xi \rightarrow 0^+$. (that is, in a small neighborhood around the the turning point) behaves almost linearly and we can expand to second-order around the Fermi energy turning-point:

$$v(x) = \epsilon_F + (x - x_F) v'_F + (x - x_F)^2 v''_F / 2 + \dots \quad (33)$$

Defining $y = (x - x_F)/l_F$ it then follows that,

$$\begin{aligned} l_F k_F(y) &= \sqrt{y} \left[1 - \chi_F y / 2 + O(y^2) \right], \\ \theta_F(y) &= \frac{2}{3} y^{3/2} \left[1 - \frac{3\chi_F y}{10} + O(y^2) \right], \\ z_F(y) &= y \left[1 - \frac{2\chi_F y}{10} + O(y^2) \right], \\ \tau_F(y)/l_F^2 &= 2y^{1/2} \left[1 + \frac{\chi_F y}{6} + O(y^2) \right]. \end{aligned} \quad (34)$$

Insertion of the above limiting forms in Eq. (18) yields the following approximation for the semiclassical densities in the vicinity of a turning point:

$$\begin{aligned} n^{\text{vic}}(x) &= \frac{1}{l_F \pi} [K_2(\theta_F) + b_F K_1(\theta_F)], \\ t^{\text{vic}}(x) &= \frac{1}{6\pi l_F^3} (K_1(\theta_F) + y [K_2(\theta_F) + b_F K_1(\theta_F)]) \end{aligned} \quad (35)$$

There are many interesting aspects to these formulas. First, they match the special case of a 1D Airy gas. Second, we see it depends on the second derivative of the potential at the turning point through the coefficient b_F . Further, taking the limit $y \rightarrow 0$ yields the previously given turning point results, Eq. (27).

We next use these formulas to derive the leading corrections to TF energies in specific spatial regions. The key observation is that the density difference from TF,

$$\Delta n(x) = n(x) - n^{\text{TF}}(x) \quad (36)$$

vanishes with some negative power of θ_F as $|x - x_F|$ becomes large in the allowed region. In the forbidden region the decay is exponential. Thus integrals over moments of this quantity are well-behaved and allows capture of the dominant energetic corrections to TF. The same remains true for the kinetic energy density.

The particle number in a given region itself provides a useful warm-up exercise. Define

$$N^{\text{forbid}} = \int_{-\infty}^{x_F} dx n(x). \quad (37)$$

Inserting the turning point vicinity density, Eq. (35), and employing the simple relations $k_F l_F \approx \sqrt{z_F}$ (from Eq. (34)) and $k dx = \sqrt{z} dz$ (valid everywhere), the integrals can be performed analytically (see appendix), to yield

$$N_\gamma^{\text{forbid}} \rightarrow N_0 - N_1 \gamma^{2/3} + \dots, \quad (38)$$

where

$$N_0 = \frac{1}{6\pi\sqrt{3}} \sim 0.03063, \quad N_1 = b_F \frac{a_0^2}{2}. \quad (39)$$

The first of these is a universal constant that applies to all turning points, while the leading correction depends on specific details, through b_F . Applying the same reasoning to the allowed region while assuming the contribution to the integrated functions at x_m is zero (which is necessarily the case when γ approaches zero), we find

$$N_\gamma^{\text{allow}} \rightarrow \frac{N}{\gamma} - N_0 + N_1 \gamma^{2/3} + \dots, \quad (40)$$

i.e., term-by-term in the γ -expansion, the gain in particle number in the evanescent region precisely cancels the loss from the allowed region. This is an explicit demonstration that the semiclassical density, which is *not* exactly normalized in general, *is* normalized to this order in the γ expansion.

A less trivial piece of information is also contained in this result. Since the TF density is entirely within the allowed region, this shows that, to leading order, approximately 0.03063 electrons leak out beyond each turning point into the neighboring evanescent region. This is a universal result for all 1D potentials, and is illustrated in Fig. 9. Even at $\gamma = 1$, the integral of the density in the forbidden region is close to the asymptotic behavior contained in Eq. (38).

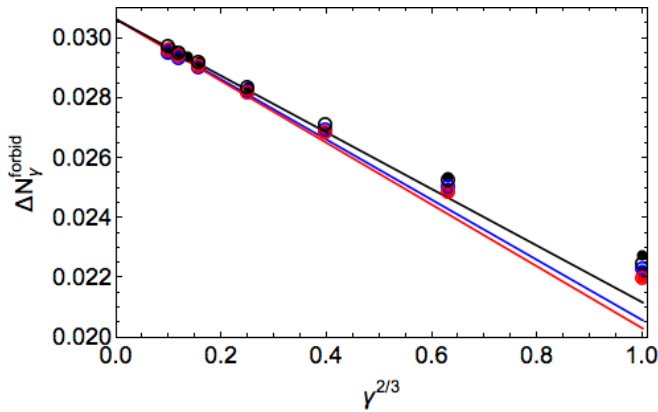


FIG. 9. N_γ^{forbid} for harmonic oscillator (black) and left- (blue) and right- (red) turning points of the Morse potential (all with $N = 1$). The straight lines are the leading asymptotic behavior as $\gamma \rightarrow 0$, given by Eq. (38). The empty circles correspond to results obtained with Eq. (21), while the filled are exact.

The approach to the semiclassical limit is illustrated in Fig. 9. It corroborates the asymptotics given by Eq. 38. In particular, inclusion of the leading corrections to the semiclassical limit yields estimates for the average number of particles in the forbidden region which are accurate to within about 10% for every case.

We also calculated the deviation from the TF result in the allowed region. In the asymptotic limit, this should

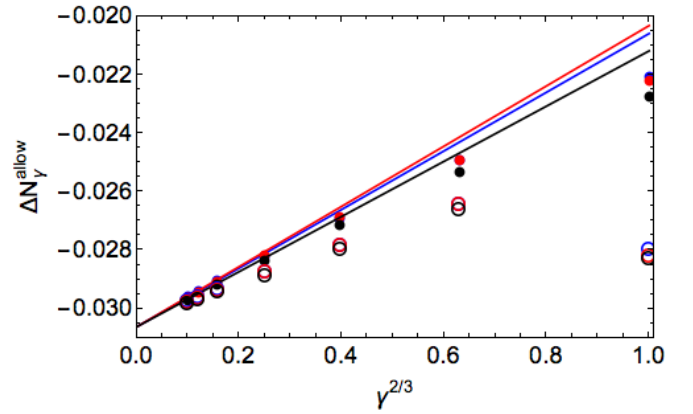


FIG. 10. Same as Fig. 9, except the deviation from N/γ in the allowed region.

become the mirror-image of the corresponding result in the evanescent region. This is shown in Fig. 10. We find that while this is true for sufficiently small γ , the deviations from straight-line behavior are much larger. This is because, e.g., for $\gamma = 1$, the integral over the appropriate K_j functions are truncated at the mid-phase point, so that only a fraction of an oscillation is included in the integration region. On the other hand, as $\gamma \rightarrow 0$, the larger number of density oscillations is averaged out, so the integral gets closer to its asymptotic value as derived in the appendix.

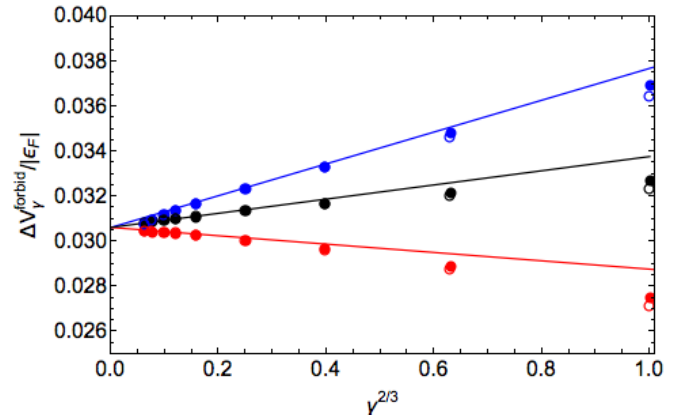


FIG. 11. Same as Fig. 9, but for $V_\gamma^{\text{forbid}}/|\epsilon_F|$.

The next simplest observable we can address is the potential energy, which is directly determined by the density. A similar analysis yields:

$$V_\gamma^{\text{forbid}} \rightarrow -\epsilon_F N_0 + \gamma^{2/3} \left(\epsilon_F N_1 + \frac{a_0^2}{10l_F^2} \right) + \dots \quad (41)$$

Thus $V_\gamma^{\text{forbid}}/\epsilon_F$ has a universal value ($-N_0$) for every potential. The average potential energy per electron in the evanescent region, is simply $-\epsilon_F$. But the correction is system-dependent. All this is illustrated in Fig. 11.

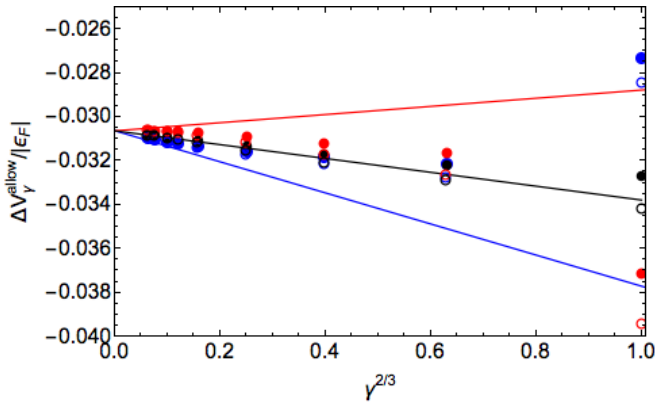
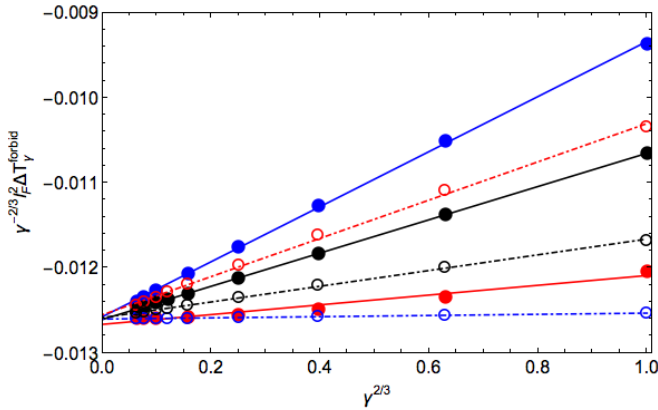


FIG. 12. Same as Fig. 11, but for the allowed region.

But, just as before, we find the change (relative to TF) in the allowed region, shown in Fig. 12, exactly cancels the contribution from the forbidden region, leaving zero contribution to the total potential energy, both for the constant contribution and the $\gamma^{2/3}$ coefficient.

FIG. 13. Same as Fig. 9, but for $l_F^2 \gamma^{-2/3} T_\gamma^{\text{forbid}}$.

Finally, we repeat the calculation for the kinetic energy, finding

$$T_\gamma^{\text{forbid}} \rightarrow -\frac{a_0^2}{10l_F^2} \gamma^{2/3} + \dots \quad (42)$$

Note the important difference relative to the previous cases: there is no constant term in Eq. (42). In Fig. 13 we illustrate how this universal limit is approached (in the evanescent region) for the Morse and harmonic oscillators. Here again, the error in the classically-allowed region is cancelled by that of the classically-forbidden.

C. Global energies

In this final subsection, we turn to global energy components. We have shown so far that, in each region of space, our semiclassical formulas reproduce the leading

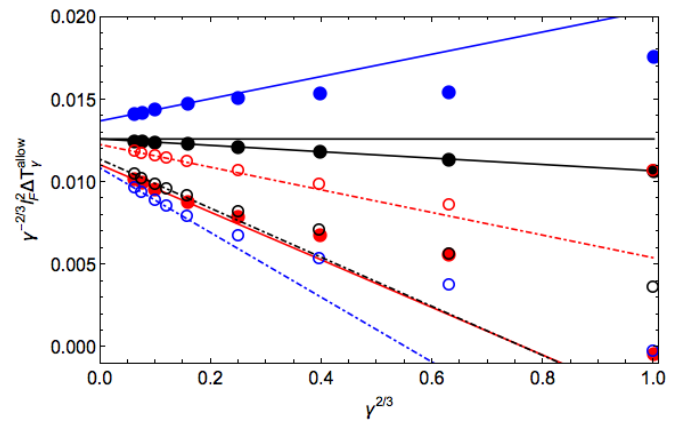


FIG. 14. Same as Fig. 13, but for the allowed region.

corrections to TF observables, often in powers of $\gamma^{1/3}$. Now we add the corrections from each region to find their effects on energy components. As we have seen, in the limit as $\gamma \rightarrow 0$, the corrections from each region cancel each other, so no net contribution from the leading-order regional contributions is left.

To understand this effect, we first consider the global integral of the density itself. While TF is defined to be normalized by construction for any $v(x)$, the semiclassical approximation is not. The particle number N enters only in defining ϵ_F , but this does not guarantee normalization. We can see this by adding Figs 9 and 10 together. While the leading corrections as $\gamma \rightarrow 0$ are given by the plotted straight lines, the deviation of the exact results from them is much greater in the allowed region than in the forbidden, implying their sum is non-vanishing. In particular, the total deviations are small and negative, as suggested by Fig. 5, being never larger than 2%. On the other hand, by construction, TF has zero error for the particle number.

While all regional contributions have $\gamma^{2/3}$ corrections to TF results, these have no effect in global properties, due to error cancellation. We find that the leading corrections to TF energies scale linearly with γ for each of the chosen potentials. The semiclassical approximations contain corrections of this order, but these are inaccurately given, as they have not been evaluated to the order needed.

Fig. 15 shows the deviation from TF values for the wells given in Table I, for both semiclassical and exact calculations. It also includes the leading corrections, which are given as straight lines. For the semiclassical approximation, these are numerical fits to a subset of the plotted points. In the case of the exact calculations, the slopes provide leading corrections to TF as determined from the exact analytic energy components given in Tables I and III. We see that in some cases, the corrections to TF are positive, while in others negative corrections are found. On the other hand, we see that the semiclassical approximation produces linear corrections, but these are not accurate. Moreover, the errors are not particu-

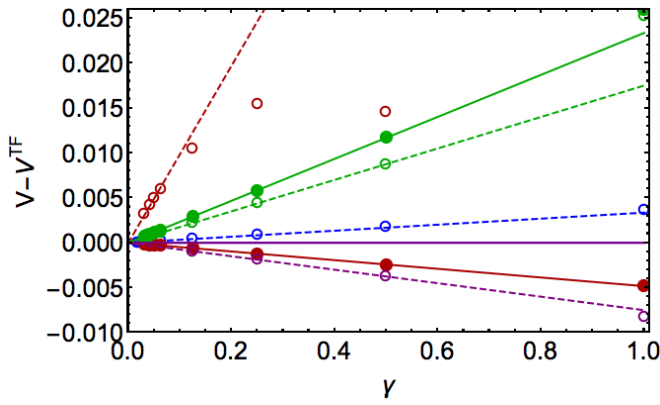


FIG. 15. $V - V^{TF}$, blue = SHO, green = quartic, red = PT, purple = Morse; empty = sc, filled = exact (when filled is not shown it is because it is zero).

larly systematic. Inclusion of higher-order corrections in terms of the potential might improve agreement with the exact curves, but that is beyond the scope of the present study.

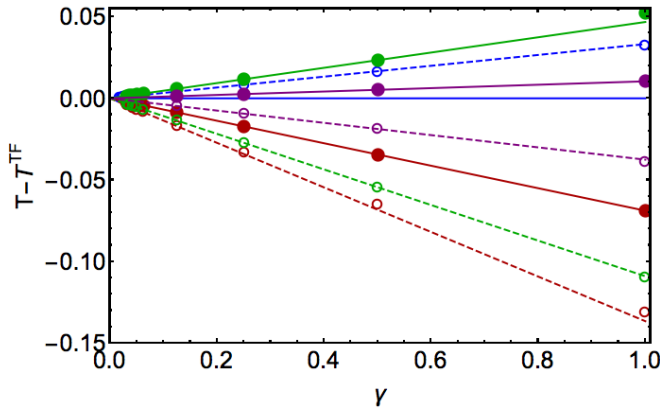


FIG. 16. $T - T^{TF}$, blue = SHO, green = quartic, red = PT, purple = Morse; empty = sc, filled = exact (when filled is not show it is because it is zero).

In Fig. 16, we find similarly baleful results for the deviations of the kinetic energy from the TF predictions. Note that these errors are typically about 5 times larger than those for the potential energy. Thus the errors for the total energy look very similar to this figure. We also note that, if we had an approximation that yielded the slopes of these curves, it would generically be very accurate, even for $\gamma = 1$. Since the TF errors change sign with different potentials, no simple gradient expansion or even a generalized gradient approximation, can hope to yield accurate corrections to TF in this limit. Such corrections remain tantalizingly out of reach at present.

We conclude that although the semiclassical uniform approximation improves over TF for all points in space, and even for each region individually as defined earlier, it does *not* yield the leading corrections to the total energies

of the system.

V. BEYOND GENERIC SITUATIONS

The potentials we have studied so far have been generic situations of particles in infinitely-differentiable wells. We have included several different situations (symmetric versus asymmetric, harmonic versus quartic) to illustrate and analyze the general behavior of the semiclassical uniform approximation especially trying to bridge the gap between its pointwise accuracy but its poorer energetic performance. The current section probes more unusual cases (one can think of many) to see what happens.

A. Limitations of semiclassical approximations

In this subsection, we explore various breakdowns of the semiclassical approximations. Before doing so, we stress that, for sufficiently smooth potentials, the semiclassical results *always* become relatively exact everywhere as $\gamma \rightarrow 0$. Here, however, we explore its application at $\gamma = 1$, i.e., not as an approach to the semiclassical limit, but instead finding systems where either the semiclassical approximations cannot be applied at all because the classical motion is unbound, or it can be used but yields relatively inaccurate results. The latter can happen if the rate of change of the potential at a Fermi energy turning point is different from zero, but very small.

Just because the semiclassical formulas can be considered as expansions around the TF limit, there is no reason to assume they are well-behaved for all potentials. We have already mentioned the fact that in general it is not normalized. We also note that it is not even guaranteed to yield densities that are positive everywhere, as the oscillations in K_1 yield negative contributions (which are much smaller than the positive contributions of K_0 everywhere unless $l_F \rightarrow \infty$).

1. Smooth potentials that vary too rapidly

A relatively trivial case that illustrates the generic breakdown of both the TF and semiclassical approaches is found by squeezing a continuous and well-behaved potential well so that it approaches a delta-well. The simplest example is the PT well, in which we take the limit where $a \rightarrow \infty$, with $D = Z/(2a)$. With this choice, the PT potential approaches $v(x) = -Z\delta(x)$. But we require

$$\beta = 1 - Na/\sqrt{2D} \quad (43)$$

to remain positive in order to define a semiclassical Fermi energy, and thus a TF or a semiclassical solution (Table I). For $a > 1$, the potential no longer bounds even one semiclassical solution, and both TF and our semiclassical approximation do not exist.

2. Hard wall limit

Another limit of considerable interest is that of hard walls, which was studied extensively in earlier work [10]. A simple method to obtain potentials of this class is by considering a symmetric potential which on the left saturates

$$\begin{aligned} v(x) &= -F(x + L/2), \quad x < -L/2 \\ &= v^{\text{box}}(x), \quad x > -L/2, \end{aligned} \quad (44)$$

where F is a constant which determines the slope of the potential, and $v^{\text{box}}(x)$ vanishes at $-L/2$ and is smooth. If we take the limit where $F \rightarrow \infty$ and $v^{\text{box}} = 0$, we recover a flat box. The Fermi energy is well-behaved in this example. However, $n^{\text{sc}}(x_F)$ (and its kinetic counterpart) is not. As $F \rightarrow \infty$, $l_F \rightarrow 0$, so that $n_F^{\text{sc}}(-L/2) \rightarrow \infty$, which is highly unphysical. The reason this happens is because of the kink in the potential at $-L/2$. As F grows, the exact density becomes *smaller* at the turning point, while the semiclassical formula diverges instead.

3. Top of the well

Two basic assumptions of the semiclassical approximations are that neither ω_F , nor v_F' vanish. Thus we expect the approximations to perform badly whenever these quantities become too small. This happens, e.g., if the semiclassical Fermi energy is close to zero for a potential that vanishes at large distances.

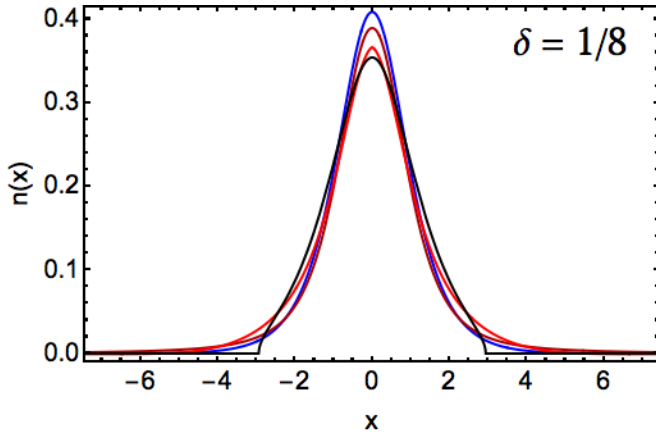


FIG. 17. Densities for PT with $D = 1/2 + 1/8$. Blue is exact, black is TF, red is semiclassical, while dark red is semiclassical with just the first contribution.

To create such an instance, we note that, while the PT potential always binds a particle when treated exactly, the semiclassical Fermi energy vanishes as $D \rightarrow 0$ (see Table I). Thus, we write $D = 1/2 + \delta$, and consider what happens as $\delta \rightarrow 0$. Figs. 17 and 18 tell the story. Even at $\delta = 1/8$, one already sees a slightly negative contribution to the density out in the tail, due to the second

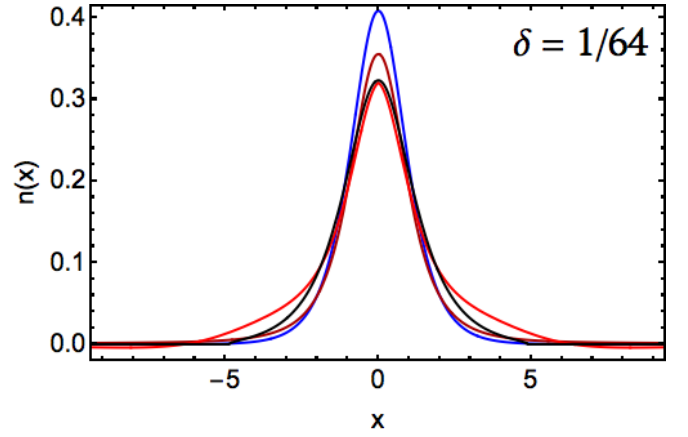


FIG. 18. Same as Fig. 17, but with $D = 1/2 + 1/64$.

term in Eq 18. We can also see that for most values of x , the semiclassical approximation is worse than TF. On the other hand, if we neglect K_1 in Eq. (20), we find a much more accurate density, without the local over and underestimates of the complete semiclassical approximation. Thus in this limit, it is better to ignore the K_1 corrections, but we note that the K_1 corrections must be included to create a uniform approximation. For sufficiently small γ , even for $\delta = 1/64$, the uniform approximation will become exact pointwise.

B. Extended systems

There is of course tremendous interest in applications of DFT to extended systems. In this section, we derive the limit of our result that applies to such systems.

For any potential of the type we have considered so far, we create a new one defined as:

$$\begin{aligned} v_L(x) &= v(x), \quad x < x_m \\ &= v(x_m), \quad x_m < x < x_m + L \\ &= v(x - L), \quad x > x_m + L. \end{aligned} \quad (45)$$

Note that this generalization depends on the value of x_m which is a function of the Fermi energy. In fact, for our purposes, we start with a given particle number N in the original well, which defines ϵ_F . We then chose $M > N$ as the number of particles in $v_L(x)$, and this defines

$$L = (M - N)\pi/k_F(x_m). \quad (46)$$

By this choice, the Fermi energy of the system containing M particles in $v_L(x)$ matches that of the N particles in $v(x)$. We now consider what happens as $M \rightarrow \infty$, so L does also. In the vicinity of the left turning point, α_F is always very small, as $\tau_F(x) \ll T_F$. Thus $\sin \alpha_F \rightarrow \alpha_F = \omega_F \tau_F(x)$. It follows that

$$d_F(x) \rightarrow \tau_F(x) k_F(x) \quad (47)$$

This is the only change needed to apply Eq. (18) to a surface problem, with a fixed chemical potential. The distant turning point has become irrelevant.

It is beyond the scope of this work to explore these surface situations, but it is of considerable interest to compare the results with e.g., those of Mattson and Kohn, and the subsequent development of density functionals using the Airy gas [28]. Our formulas yield quantum oscillations that typically extend deeply into the bulk (i.e., for $x > x_m$) and moreover, as $\gamma \rightarrow 0$, the results in a neighborhood of the surface depend on v_F'' , i.e., the Fermi-level curvature. On the other hand, as we have seen, none of these effects necessarily contribute to the energy.

C. Tunneling

Here, we generalize our approximations to the case where more than two turning points exist for the Fermi energy, by simply treating each well independently. Our aim is to study the accuracy of the semiclassical formulae for densities penetrating barriers. A simple case is given by a double well with

$$v(x) = \frac{1}{2} \left(x^2 - \frac{b^2}{4} \right)^2, \quad (48)$$

with b positive. In particular we check the local and energetic corrections to TF for two “bond lengths” (distance between the minima of the studied potential).

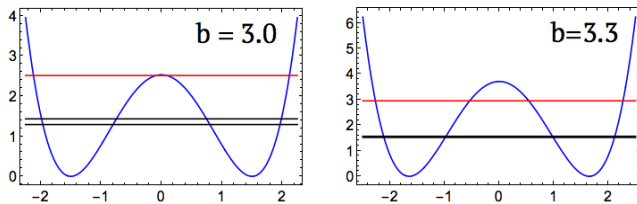


FIG. 19. Double well potentials (blue) with near degenerate eigenstates (black) and Fermi level (red) for $b = 3.0$ in Eq. (48) and for $b = 3.3$.

In Fig. 19, we show a generic case of a potential with a substantial barrier separating two wells. On the r.h.s $b = 3.3$, and the exact eigenvalues are almost degenerate, while the semiclassical Fermi energy is not close to the top of the barrier. Fig. 20 shows our usual excellent results for the densities in this case. In the evanescent region near each turning point, the semiclassical formula is extremely accurate. It fails only near the midpoint, $x = 0$, as expected. At $x = 0$ and nearby, contributions from left and right wells interfere with each other, and our approximation does not include such effects. In Fig. 21, we see that the semiclassical kinetic energy density shares these traits, though deviations from the exact result are larger, as expected.

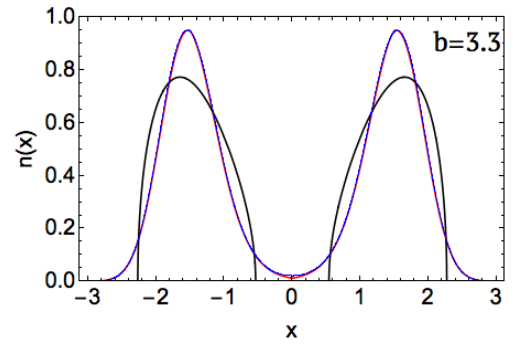


FIG. 20. Particle density (blue is exact, red is semiclassical, black is TF) for the double well of Fig. 19 with $b = 3.3$.

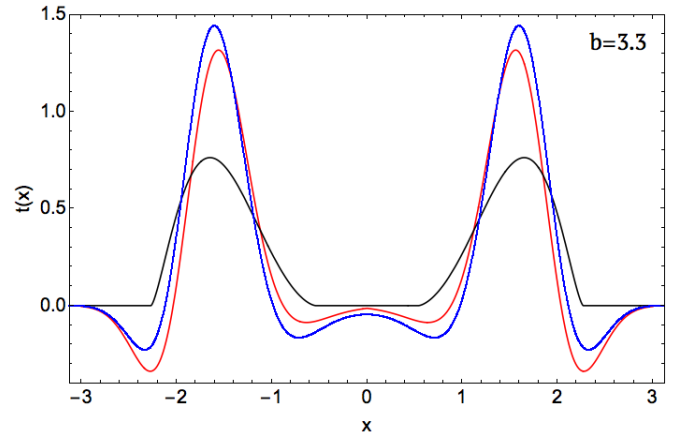
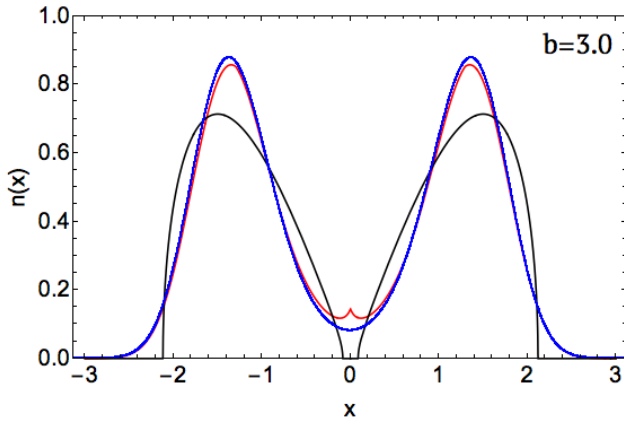
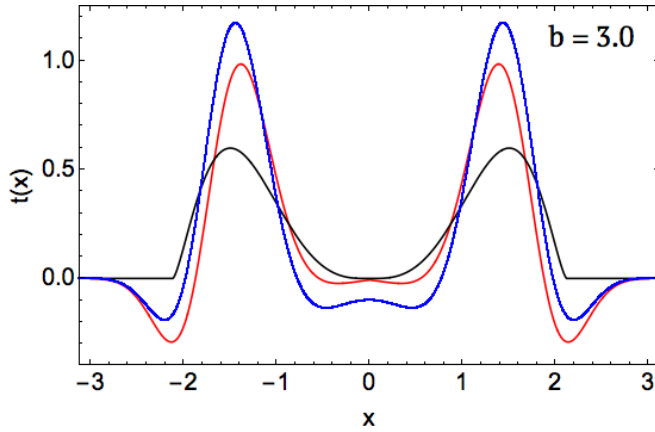


FIG. 21. Same as Fig. 20, but for kinetic energy density.

Even when we reduce the separation b to a smaller distance, pushing ϵ_F to almost the top of the barrier, as shown on the l.h.s of Fig. 19, thus creating the conditions of Sec V A 3, the semiclassical approximations continue to perform well. The density is plotted in Fig. 22, and comparable quality is achieved for the kinetic energy as is shown in Fig. 23.

VI. CONCLUSIONS

This paper explores in considerable detail the performance of the uniform semiclassical approximations for the particle- and kinetic-energy densities first presented in Ref. [13]. A large variety of properties have been found analytically and been tested numerically for a diverse set of potentials (all infinitely differentiable). By defining regional contributions to particle number and energy components, we show that the spectacular pointwise accuracy of the semiclassical approximations does transfer to integrals over spatial domains. But we also showed how the contributions from the semiclassical corrections vanish when integrated globally, so that these contributions are *not* the leading corrections to energy

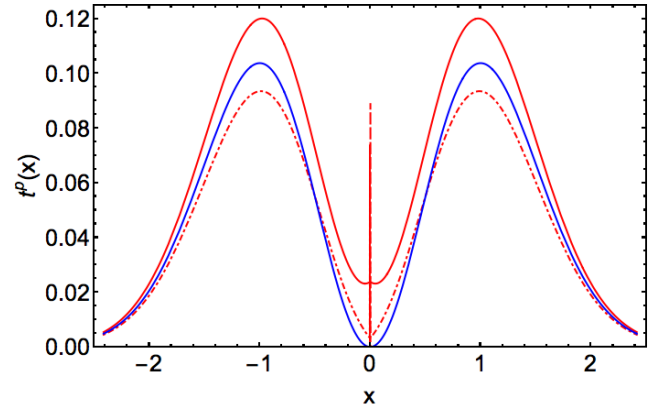
FIG. 22. Same as Fig. 20, but for $b = 3.0$.FIG. 23. Same as Fig. 21, but for $b = 3.0$.

components.

There are many extensions of this work that have only been mentioned or superficially pursued here. One such is the derivation of semiclassical approximations which accurately describe the tunneling region between different wells. This should be uniformly accurate for all values of x . Another concerns a more detailed study of double wells, e.g., checking how accurate the uniform semiclassical approximations are in the multiple well case relative to the case of a single. An additional relevant extension of this work could be obtained by generalizing the treatment here given to 3D systems that are uniform in two directions, but vary in a third. Such would be useful for the study of quantum dots, cold-atom fermion traps, and plasma physics (when generalized to high temperatures) [29]. Yet one more important area is surface energies. We have generalized but not tested the corresponding semiclassical approximations for such problems, where regional properties do matter very much.

Lastly, we discuss the relevance of these results to density functional theory [30]. Of greatest interest is the pursuit of a non-interacting kinetic energy functional of the density, often referred to as allowing orbital-free DFT

[31]. In general, it has been found that, for interacting 3D electronic systems, the 2nd-order gradient expansion for the kinetic energy is highly accurate [30], but higher orders often worsen properties [8]. Here, we have shown that functionals of the potential that go beyond the local approximations can be extremely accurate pointwise, while showing no systematic improvement globally. This indeed mimics experience in the real 3D world, where pointwise agreement can be greatly improved in 4th order, without corresponding global improvement [32]. All this deepens further the mystery of the difficult relationship between potentials and densities for fermionic systems [20]. We have also found that, in order to recover the leading regional corrections to TF results, the slope of the potential at the turning point is insufficient, and that the next derivative contributes substantially to these corrections. This appears important for the construction of approximate functionals using the Airy gas [27, 28, 33]. Again, there are obvious further extensions of this work. For example, does the local density approximation, applied to either the exact or the semiclassical density, yield more accurate pointwise and regional properties than when applied to its self-consistent density? Can any of the potential functional approximations given here be converted to simple density functional forms, that capture their energetic consequences?

FIG. 24. Positive kinetic energy $t^p(x)$: Exact (blue), semiclassical (dot-dashed red), semiclassical without higher-order terms in γ (continuous red).

Finally, we mention the choice of kinetic energy density used in this work. Our choice is a natural one starting from semiclassical analysis since it assigns a local orbital kinetic energy $|\phi_i(x)|^2 p_i^2(x)/2$, where $p_i(x) = \epsilon_i - v(x)$, to each occupied state of the system. Thus it is directly analogous to the classical kinetic energy density of a configuration space distribution of particles with energy ϵ_i .

But the purely positive choice has become popular in DFT, especially for the construction of meta-GGA's [2]. They are related via

$$t^{\text{pos}}(x) = \frac{1}{2} \sum_{i=1}^N \int dx \left| \frac{d\phi_i}{dx} \right|^2 = t(x) + \frac{1}{4} \frac{d^2 n}{dx^2}. \quad (49)$$

Thus we can use Eq. (18) to construct approximations for $t^{\text{pos}}(x)$, and these are plotted for the harmonic oscillator with 1 particle in Fig. 24. We see that the accuracy of the approximations to $t^{\text{pos}}(x)$ is similar to those for $t(x)$ in Fig 4, apart from the mid-phase point. There the small kink in the semiclassical approximation for $n(x)$ has its effects magnified by the two derivatives of the density which must be taken in order to evaluate $t^{\text{pos}}(x)$. However, the resulting analytic expression for the positive kinetic energy density includes derivatives up to second-order in the potential, unlike the expressions of Eq. (18) which contain none. These can be shown to be irrelevant as $\gamma \rightarrow 0$. Furthermore, because n^{sc} and t^{sc} are only guaranteed to include the leading corrections to TF, the terms involving high powers of γ which emerge from $d^2 n^{sc}(x)/dx^2$ are likely incorrect. Thus, we also construct an approximation for the positive kinetic energy density in which all such higher-derivative terms are neglected. This is shown by the dashed line in Fig. 24. As expected, it is substantially more accurate than the semiclassical approximation obtained for t^{pos} which does not remove higher-order terms of the γ expansion. Hence use of $t^{\text{pos}}(x)$ in this way either involves more complicated analytic expressions or a loss of accuracy.

To summarize, we have explored the accuracy of uniform semiclassical approximations to both the particle and kinetic energy densities of noninteracting fermions in 1d, finding (unfortunately) that their spectacular performance pointwise in improvement over TF results does *not* translate directly to improved energy components. This is explained by the difference between regional corrections to the energy and global averages. Limitations of the semiclassical approximations have been explored and the relevance to density functional theory discussed.

We gratefully acknowledge support of the NSF through grant number CHE-1464795.

VII. APPENDIX - RELEVANT PROPERTIES OF AIRY FUNCTIONS

A. Definitions

We define the following notation for pairs of Airy functions

$$A_0 = -aa', \quad A_1 = a^2, \quad A_2 = a'^2, \quad (50)$$

where $a(z) = Ai(-z)$ and $a' = da/dz$. From these, we define the combinations relevant to this work:

$$\begin{aligned} K_2(z) &= \pi [zA_1(z) + A_2(z)], \\ K_1(z) &= \pi A_0(z), \\ K_0(z) &= z^{-3/2} \left[zK_2(z) - \frac{K_1(z)}{2} \right], \end{aligned} \quad (51)$$

Next we list the asymptotic expansions of $A_i(z)$ in the three regions with qualitatively different behavior. In the

traveling region,

$$\begin{aligned} \pi z^{\pm 1/2} A_{1,2}(z) &\rightarrow \frac{1 \pm \sin(2\theta)}{2} - \frac{(1 \mp 6)\cos(2\theta)}{72\theta} + \dots, \\ \pi A_0(z) &\rightarrow -\frac{\cos(2\theta)}{2} + \frac{6 + \sin(2\theta)}{72\theta} + \dots \end{aligned} \quad (52)$$

In the classically-forbidden region

$$\begin{aligned} |z|^{\pm 1/2} A_{1,2}(z) &\rightarrow \frac{e^{-2|\theta|}}{4} \left(1 + \frac{1 \mp 6}{36|\theta|} + O(|\theta|^{-2}) \right), \\ \pi A_0(z) &\rightarrow -\frac{e^{-2|\theta|}}{4} \left(1 + \frac{1}{36|\theta|} + O(|\theta|^{-2}) \right) \end{aligned} \quad (53)$$

In a small neighborhood of some turning point,

$$\begin{aligned} A_1(z) &\rightarrow a_0^2 + \frac{z}{\pi\sqrt{3}} + O(z^2), \\ A_2(z) &\rightarrow \frac{1}{12\pi^2 a_0^2} - \frac{z^2}{2\pi\sqrt{3}} + O(z^3), \\ A_0(z) &\rightarrow -\frac{1}{2\sqrt{3}\pi} + \frac{z}{12\pi^2 a_0^2} + O(z^2), \end{aligned} \quad (54)$$

where

$$a_0 = a(0) = \frac{3^{-2/3}}{\Gamma(2/3)} = 0.35028. \quad (55)$$

Now we combine the results above to obtain asymptotic approximations to the K_i functions In the traveling region,

$$\begin{aligned} K_1(z) &\rightarrow -\frac{\cos(2\theta)}{2} + \frac{6 + \sin(2\theta)}{72\theta} + O(\theta^{-2}), \\ K_0(z) &\rightarrow 1 + O(\theta^{-2}), \\ K_2(z) &\rightarrow \left(\frac{3\theta}{2} \right)^{1/3} \left[1 - \frac{\cos(2\theta)}{6\theta} + O(\theta^{-2}) \right]. \end{aligned} \quad (56)$$

In the evanescent,

$$\begin{aligned} K_1(z) &\rightarrow -\frac{e^{-2|\theta|}}{4} \left[1 + \frac{1}{36|\theta|} + O(|\theta|^{-2}) \right], \\ K_0(z) &\rightarrow -\frac{e^{-2|\theta|}}{2} [1 + O(|\theta|^{-2})], \\ K_2(z) &\rightarrow \frac{e^{-2|\theta|}}{2} \left(\frac{3|\theta|}{2} \right)^{1/3} \left[1 - \frac{1}{6|\theta|} + O(|\theta|^{-2}) \right] \end{aligned} \quad (57)$$

Near a turning point,

$$\begin{aligned} K_1(z) &\rightarrow -\frac{1}{2\sqrt{3}} + \frac{z}{12\pi a_0^2} + O(z^2), \\ K_0(z) &\rightarrow z^{-3/2} \left[\frac{1}{4\sqrt{3}} + \frac{z}{24\pi a_0^2} + O(z^2) \right], \\ K_2(z) &\rightarrow \frac{1}{12\pi a_0^2} + \pi a_0^2 z + O(z^2). \end{aligned} \quad (58)$$

These were used to derive Eq. (27) of the text.

Finally, in obtaining corrections to TF in the forbidden regions, we evaluated a variety of integrals of Airy

functions. Here we show those which are needed to verify our results. Defining

$$I_p^m = \int_0^\infty dz z^m K_p(z), \quad (59)$$

then it follows that [34],

$$I_2^0 = -\frac{1}{6\sqrt{3}}, \quad I_1^0 = \frac{\pi a_0^2}{2}, \quad I_2^1 = \frac{I_1^0}{5}, \quad I_1^1 = -\frac{1}{24\pi a_0^2}. \quad (60)$$

To repeat the calculation in the allowed region, one must subtract the corresponding TF values (the dominant terms in Eq. (56)) from the K_i functions to find the deviations from TF. These allow verification of Eqs. (38-42) of the text.

-
- [1] Aurora Pribram-Jones, David A. Gross, and Kieron Burke, “Dft: A theory full of holes?” *Annual Review of Physical Chemistry* **66**, 283–304 (2015).
 - [2] Jianwei Sun, Adrienn Ruzsinszky, and John P. Perdew, “Strongly constrained and appropriately normed semilocal density functional,” *Phys. Rev. Lett.* **115**, 036402 (2015).
 - [3] L. H. Thomas, “The calculation of atomic fields,” *Math. Proc. Camb. Phil. Soc.* **23**, 542–548 (1927).
 - [4] E. Fermi, “Eine statistische Methode zur Bestimmung einiger Eigenschaften des Atoms und ihre Anwendung auf die Theorie des periodischen Systems der Elemente (a statistical method for the determination of some atomic properties and the application of this method to the theory of the periodic system of elements),” *Zeitschrift für Physik A Hadrons and Nuclei* **48**, 73–79 (1928).
 - [5] Elliott H. Lieb and Barry Simon, “Thomas-fermi theory revisited,” *Phys. Rev. Lett.* **31**, 681–683 (1973).
 - [6] Kieron Burke, Antonio Cancio, Tim Gould, and Stefano Pittalis, “Locality of correlation in density functional theory,” *The Journal of Chemical Physics* **145**, 054112 (2016), <http://dx.doi.org/10.1063/1.4959126>.
 - [7] P. Elliott, D. Lee, A. Cangi, and K. Burke, “Semiclassical origins of density functionals,” *Phys. Rev. Lett.* **100**, 256406 (2008).
 - [8] Donghyung Lee, Lucian A. Constantin, John P. Perdew, and Kieron Burke, “Condition on the kohn–sham kinetic energy and modern parametrization of the thomas–fermi density,” *J. Chem. Phys.* **130**, 034107 (2009).
 - [9] Peter Elliott and Kieron Burke, “Non-empirical derivation of the parameter in the b88 exchange functional,” *Can. J. Chem. Ecol.* **87**, 1485–1491 (2009).
 - [10] A. Cangi, D. Lee, P. Elliott, and K. Burke, “Leading corrections to local approximations,” *Phys. Rev. B* **81**, 235128 (2010).
 - [11] L. A. Constantin, J. Snyder, J. P. Perdew, and K. Burke, “Ionization potential in the limit of large atomic number,” *J. Chem. Phys.* **133**, 241103 (2011).
 - [12] A. Cangi, E. K. U. Gross, and K. Burke, “Potential functionals versus density functionals,” *Phys. Rev. A* **88**, 062505 (2013).
 - [13] Raphael F. Ribeiro, Donghyung Lee, Attila Cangi, Peter Elliott, and Kieron Burke, “Corrections to thomas-fermi densities at turning points and beyond,” *Phys. Rev. Lett.* **114**, 050401 (2015).
 - [14] Raphael F. Ribeiro and Kieron Burke, “Uniform semiclassical approximations for one-dimensional fermionic systems,” *arXiv preprint arXiv:1510.05676* (2015).
 - [15] G. Wentzel, “Eine verallgemeinerung der quantenbedingungen für die zwecke der wellenmechanik,” *Z. Phys.* **38**, 518 (1926).
 - [16] H.A. Kramers, “Wellenmechanik und halbzahlige quantisierung,” *Z. Phys.* **39**, 828 (1926).
 - [17] L. Brillouin, “La mecanique ondulatoire de schrödinger: une methode generale de resolution par approximations successives,” *Compt. Rend.* **183**, 24 (1926).
 - [18] R. E. Langer, “On the connection formulas and the solutions of the wave equation,” *Phys. Rev.* **51**, 669–676 (1937).
 - [19] Adam Wasserman, Jonathan Nafziger, Kaili Jiang, Min-Cheol Kim, Eunji Sim, and Kieron Burke, “The importance of being self-consistent,” *Annual Review of Physical Chemistry* **68** (2017), 10.1146/annurev-physchem-052516-044957.
 - [20] E. H. Lieb, “Thomas-fermi and related theories of atoms and molecules,” *Rev. Mod. Phys.* **53**, 603–641 (1981).
 - [21] S. Fournais, M. Lewin, and J. P. Solovej, “The semiclassical limit of large fermionic systems,” *ArXiv e-prints* (2015), [arXiv:1510.01124](https://arxiv.org/abs/1510.01124) [math-ph].
 - [22] Attila Cangi, Donghyung Lee, Peter Elliott, Kieron Burke, and E. K. U. Gross, “Electronic structure via potential functional approximations,” *Phys. Rev. Lett.* **106**, 236404 (2011).
 - [23] Mohandas Pillai, Joshua Goglio, and Thad G Walker, “Matrix numerov method for solving schrödingers equation,” *American Journal of Physics* **80**, 1017–1019 (2012).
 - [24] Wolfram Research, Inc., “*Mathematica*,” (2015).
 - [25] N. H. March and J. S. Plaskett, “The relation between the wentzel-kramers-brillouin and the thomas-fermi approximations,” *Proceedings of the Royal Society of London. Series A. Mathematical and Physical Sciences* **235**, 419–431 (1956).
 - [26] W. Kohn and L. J. Sham, “Quantum density oscillations in an inhomogeneous electron gas,” *Phys. Rev.* **137**, A1697–A1705 (1965).
 - [27] W. Kohn and A. E. Mattsson, “Edge electron gas,” *Phys. Rev. Lett.* **81**, 3487 (1998).
 - [28] A. Lindmaa, A. E. Mattsson, and R. Armiento, “Quantum oscillations in the kinetic energy density: Gradient corrections from the airy gas,” *Phys. Rev. B* **90**, 075139 (2014).
 - [29] Attila Cangi and Aurora Pribram-Jones, “Efficient formalism for warm dense matter simulations,” *Physical Review B* **92**, 161113 (2015).
 - [30] R. M. Dreizler and E. K. U. Gross, *Density Functional Theory: An Approach to the Quantum Many-Body Problem* (Springer-Verlag, Berlin, 1990).
 - [31] Y. A. Wang and E. A. Carter, “Orbital-free kinetic-

- energy density functional theory,” in *Theoretical Methods in Condensed Phase Chemistry*, edited by S. D. Schwartz (Kluwer, Dordrecht, 2000) Chap. 5, p. 117.
- [32] John P Perdew and Lucian A Constantin, “Laplacian-level density functionals for the kinetic energy density and exchange-correlation energy,” *Physical Review B* **75**, 155109 (2007).
- [33] R. Armiento and A.E. Mattsson, “Functional designed to include surface effects in self-consistent density functional theory,” *Phys. Rev. B* **72**, 085108 (2005).
- [34] Olivier Vallee and Manuel Soares, *Airy Functions and Applications to Physics* (Imperial College Press, London, 2004).